

Solid-State NMR and MD Simulations of the Antiviral Drug Amantadine Solubilized in DMPC Bilayers

Conggang Li,^{*†} Myunggi Yi,^{‡§¶} Jun Hu,^{*†} Huan-Xiang Zhou,^{‡§¶} and Timothy A. Cross^{*†¶}

^{*}Department of Chemistry and Biochemistry, [†]National High Magnetic Field Laboratory, [‡]Department of Physics, [§]Institute of Molecular Biophysics, and [¶]School of Computational Science, Florida State University, Tallahassee, Florida

ABSTRACT The interactions of ¹⁵N-labeled amantadine, an antiinfluenza A drug, with DMPC bilayers were investigated by solid-state NMR and by a 12.6-ns molecular dynamics (MD) simulation. The drug was found to assume a single preferred orientation and location when incorporated in these bilayers. The experimental and MD computational results demonstrate that the long axis of amantadine is on average parallel to the bilayer normal, and the amine group is oriented toward the headgroups of the lipid bilayers. The localization of amantadine was determined by paramagnetic relaxation and by the MD simulation showing that amantadine is within the interfacial region and that the amine interacts with the lipid headgroup and glycerol backbone, while the hydrocarbon portion of amantadine interacts with the glycerol backbone and much of the fatty acyl chain as it wraps underneath the drug. The lipid headgroup orientation changes on drug binding as characterized by the anisotropy of ³¹P chemical shielding and ¹⁴N quadrupolar interactions and by the MD simulation.

INTRODUCTION

Like many other drugs, amantadine, which inhibits conductance by the M2 proton channel from influenza virus, is lipophilic. The ability of drugs to cross hydrophobic barriers to reach their targets will affect their pharmacokinetics and toxicology. The partitioning of drugs into membranes not only influences drug transport, distribution, selectivity, and efficiency but also alters the physical properties of membranes (1–3). In addition, many lipophilic ligands partitioning into membranes appear to have a preferred location and orientation that facilitates interactions with receptors through lateral diffusion (3,4). Thus, the characterization of drug interactions with membranes is important for further drug development. Here, the interaction of amantadine with a lipid bilayer is characterized by solid-state NMR and by molecular dynamics (MD) simulation.

Amantadine (1-aminoadamantane) is a licensed drug that has been used for the prophylaxis and treatment of influenza A viral infections. The target of amantadine is the M2 proton channel, which is critical for viral replication (5,6). The M2 protein has 96 residues with a single 19-residue transmembrane helix. The functional structure of the M2 channel is minimally tetrameric (5). Electrophysiological studies demonstrate that the M2 protein selectively conducts protons through a variety of membrane systems, such as the oocytes of *Xenopus laevis* (7), mammalian cells (8), and planar lipid bilayers (9). Significant suppression of proton conductance by amantadine or rimantadine in these systems is well documented (10,11). The transmembrane domain of M2 (M2-TMD) also forms a proton-selective channel in lipid bilayers that is sensitive to

amantadine (12). However, the mechanism by which amantadine compromises M2 proton conductance is still controversial. Most frequently, amantadine is regarded as a channel blocker. Alternatively, it may act as an allosteric inhibitor by which amantadine binds outside the pore region and presumably from the lipid environment, thereby inducing a conformational change to the channel and inducing closure of the channel. In addition, it has recently been speculated that amantadine may interfere with the channel mechanisms by which protons are conducted (13,14). Amantadine and its derivatives have also been studied as possible drugs against the human immunodeficiency virus-1 (HIV-1) and Parkinson's disease (15,16).

A variety of biophysical methods, including neutron and x-ray diffraction (17), solution NMR (18), and EPR (19), have been applied to study the association between amantadine and cellular membranes. The partition coefficient of a spin-labeled amantadine analog in 1,2-dimyristoyl-*sn*-glycero-3-phosphocholine (DMPC) vesicles, measured by EPR, is 11.2 at 45°C (19), whereas the partition coefficient of amantadine in DMPC/1,2-dihexanoyl-*sn*-glycero-3-phosphocholine (DHPC) bicelles, measured by a solution NMR diffusion method, is 27.6 (18). It is therefore clear that amantadine has a high affinity for membranes while having significant solubility in the aqueous phase. Neutron and x-ray diffraction studies (17) indicate that a majority of the drug occupies a region around the headgroups of DOPC, although these diffraction studies appear to suggest that a portion of these molecules bind near the bilayer center. On the other hand, the drug was found to be around phosphate groups as well as the hydrocarbon chains by saturation transfer difference experiments in solution NMR (18).

Orientation-dependent spin interactions can be observed by solid-state NMR from uniformly aligned samples; this provides restraints on the orientation of the observed molecular

Submitted May 10, 2007, and accepted for publication August 21, 2007.

Address reprint requests to Timothy A. Cross, National High Magnetic Field Laboratory, Florida State University, Tallahassee, FL 32310. Tel.: 1-850-644-0917; Fax: 1-850-644-1366; E-mail: cross@magnet.fsu.edu.

Editor: Anthony Watts.

site, and data on motional averaging can be obtained from unoriented samples. In addition, water-soluble relaxation agents can be added to the membrane samples to characterize the depth of a molecular site within the membrane environment. Here, we describe the alignment, location, and charge state of amantadine in DMPC bilayers and the influence of amantadine on these bilayers. Solid-state NMR methods and MD simulation will be used as two approaches that provide highly complementary insights.

MATERIALS AND METHODS

Materials

The ^{15}N -amantadine-HCl was synthesized according to published procedures (20). ^{15}N -labeled acetonitrile (Isotech, Miamisburg, Ohio) was used to provide the ^{15}N source. The final product was verified by mass and ^1H solution NMR spectroscopy.

Oriented samples of hydrated DMPC bilayers were prepared by first dissolving DMPC (100 mg) in 5 ml trifluoroethanol (TFE). TFE was removed by rotary evaporation and dried under high vacuum, and 15 ml of 20 mM citrate-borate-phosphate (CBP) buffer ($\sim 37^\circ\text{C}$, pH 8.0) with 1 mM ethylenediamine tetra-acetic acid (EDTA) was added to the dried mixture and shaken at 37°C . This lipid suspension was bath sonicated for 10 min intermittently. The sonicated suspension was loaded into a 3 kDa MW cutoff dialysis bag. The dialysis bag was placed in 1 liter of 20 mM CBP buffer overnight to adjust the pH of liposomes. For a sample with amantadine, a desired concentration of amantadine-HCl (Fisher Scientific, GA) in 5 ml CBP buffer was added to the DMPC vesicle suspension (20 ml). The suspension was incubated at room temperature overnight and pelleted in 2.5 h by ultracentrifugation at $196,000 \times g$. The pH value of the pellet was inferred from a measurement of the supernatant. The pellet was agitated at 37°C for 1 h until it became fluid. This viscous fluid was spread onto 50 glass slides ($5.7 \text{ mm} \times 12.0 \text{ mm}$) (Marienfeld Glassware, Bad Margentheim, Germany) and dried in a humidity (70–75% relative humidity) chamber using a N_2 atmosphere. The dehydrated slides were stacked together, inserted into a glass tube, and rehydrated in a 96% humidity (saturated K_2SO_4) chamber at 40°C for 1 wk. The resultant sample had between 20 and 30 waters/lipid molecule. Finally, the glass tube was sealed.

NMR experiments

Static ^{31}P NMR experiments were conducted on a Bruker DMX-300 at 303 K using an NHMFL $^{31}\text{P}/^1\text{H}$ double resonance probe, and H_3PO_4 was used as a reference for 0 ppm. ^{15}N NMR experiments were performed on a 400 MHz spectrometer using an NHMFL static $^{15}\text{N}/^1\text{H}$ probe with a flat coil. Typically, an 800- μs cross-polarization contact time, 6-s recycle delay, and 50-kHz B_1 field for both the ^1H and ^{15}N channels were used. The ^{15}N chemical shift was referenced to $^{15}\text{NH}_4\text{NO}_3$ at 26 ppm relative to liquid ammonia. The ^{14}N spectra were obtained using a quadrupolar echo sequence (21) on an 830-MHz spectrometer at room temperature with an NHMFL probe. ^{13}C MAS NMR were performed on a 300-MHz wide-bore spectrometer with a 4-mm double-resonance Bruker MAS probe operated at a spinning frequency of 6 kHz and a temperature of 303 K.

MD simulation

The MD simulation was performed using AMBER 8 (22). Because AMBER does not have force field parameters for the DMPC lipid molecule, CHARMM27 parameters (23) were employed for the lipid in the simulations. The charges for amantadine were developed using Gaussian 03 (24) and the restraint electrostatic potential (RESP) fitting method (25) (Table 1),

TABLE 1 Partial charges of amantadine by *ab initio* and RESP combined calculations

Atom	Charge	Atom	Charge
N	-1.12499	H_N	0.37895
C_α	0.79573		
C_β	-0.37719	H_β	0.06968
C_γ	-0.3982	H_γ	0.08143
C_δ	0.35686	H_δ	-0.02657

and topology parameters were assigned according to the general AMBER force field (26). The average temperature was maintained at 310 K (above the DMPC phase transition temperature, 296 K) with a 2-ps coupling time constant, and the average pressure was maintained at 1 bar with anisotropic scaling and a 2-ps relaxation time (27). The periodic boundary condition was enforced. The nonbonded cutoff was set to 9.0 Å, and the nonbonded list was updated with a 2.0-Å skin width. The particle mesh Ewald method (28–30) was applied to calculate long-range electrostatic interactions. All bond lengths involving hydrogen were constrained with SHAKE and RATTLE algorithms (31,32), allowing an integration time step of 2 fs. The coordinates were saved every 1 ps for analysis.

The simulated system consisted of one amantadine molecule and 68 DMPC lipid molecules (34 DMPC molecules in each leaflet), forming a hydrated bilayer with 3014 TIP3P (33) water molecules. Initially the amantadine molecule was placed near the center of the preequilibrated bilayer (courtesy of Turgut Bastug (34)). To start the simulation, the system was energy minimized with gradually decreasing harmonic restraints to remove bad contacts. The system was then heated to 310 K for 40 ps at constant volume. Thereafter, the simulation was continued at constant temperature and pressure for 12.6 ns. The last 10 ns of the trajectory was analyzed for this study (see Fig. 6).

RESULTS

Charged state of amantadine in DMPC bilayers

As indicated in Fig. 1, for a sample of ^{15}N -labeled amantadine in hydrated DMPC bilayers prepared at pH 2.0, the static ^{15}N signal was distinguished by an apparent isotropic resonance around 64 ppm. The spectrum at pH 8.0 displayed a typical axially symmetric powder pattern, with $\sigma_\perp = 49$ ppm and $\sigma_\parallel = 66$ ppm. We ascribe the signal at pH 2.0 to the positively charged amantadine in which the primary amine has very little chemical shift anisotropy and a changed isotropic average. The broadening of the symmetric resonance may be the result of chemical exchange. At pH 8.0, the amantadine is a free base leading to a significant chemical shift anisotropy. Throughout this article, results at pH 8.0, involving the neutral instead of charged form of amantadine, are reported.

The alignment of amantadine in DMPC bilayers

Macroscopically aligned NMR samples were prepared at pH 8.0, and the orientations of the phospholipid bilayers on the glass plates were characterized by ^{31}P -NMR shown in the left column of Fig. 2. The molar ratio of amantadine to lipid is 1:20. The ^{31}P and ^{15}N spectra of an unoriented sample (Fig. 2, *A* and *D*, respectively) show typical powder pattern

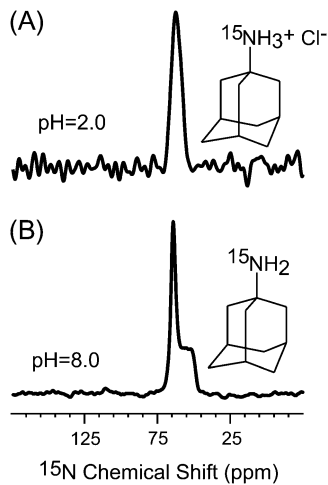


FIGURE 1 Static ^{15}N spectra of amantadine in hydrated randomly oriented DMPC bilayers at pH 2.0 (A) and pH 8.0 (B) at 30°C in a 400-MHz spectrometer.

spectra, implying a homogeneous sample preparation. When the sample was aligned between glass plates and oriented with the bilayer normal perpendicular to the magnetic field direction, the ^{31}P resonance was observed at approximately -18 ppm (Fig. 2 B), and the ^{15}N resonance from amantadine was observed to be close to 69 ppm (Fig. 2 E). When the sample was rotated by 90° such that the bilayer normal was parallel to the magnetic field, the ^{31}P resonance shifted to 36 ppm (Fig. 2 C), and the ^{15}N resonance shifted to 50 ppm (Fig. 2 F). The results indicate that the amantadine takes on a preferential orientation and does not rotate isotropically in the membrane. The resonances in the aligned sample

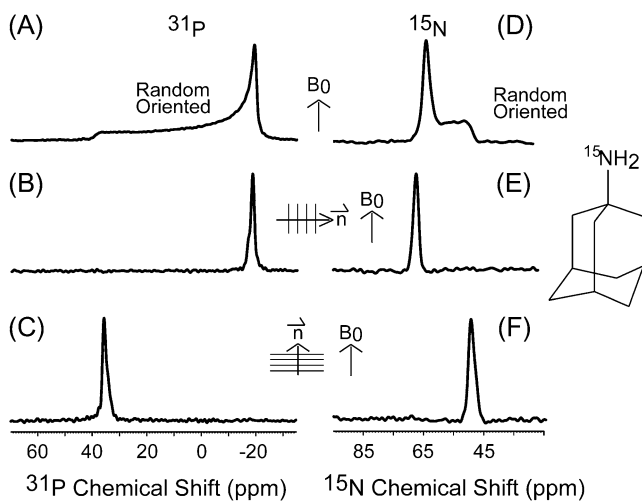


FIGURE 2 Static ^{31}P spectra (left column) of DMPC using 300-MHz spectrometer and ^{15}N spectra (right column) of amantadine in hydrated DMPC bilayers using 400-MHz spectrometer: (A and D) no alignment, (B and E) perpendicular, and (C and F) parallel with respect to the static magnetic field (B_0). The experiments were performed at 30°C and pH 8.0. The molar ratio of amantadine to lipid is 1:20.

correspond approximately to parallel and perpendicular values of the powder sample, indicating that amantadine is rotating rapidly about the bilayer normal on the chemical shift time scale.

Influence of amantadine on the dynamics and orientation of phospholipid headgroups

^{31}P and ^{14}N NMR spectra were recorded to probe directly the zwitterionic $\text{P}^--\text{O}-\text{CH}_2-\text{CH}_2-\text{N}^+(\text{CH}_3)_3$ headgroup electric dipole of DMPC. Such spectra of DMPC/amantadine liposomes at different molar ratios are shown in Fig. 3. In pure DMPC bilayers, the chemical shift anisotropy (CSA, $\sigma_{\parallel} - \sigma_{\perp}$) of ^{31}P was 47 ppm (Fig. 3 A), and the quadrupolar splitting (measured as the separation of the ν_{\perp} components) of the choline group of DMPC was ~ 11 kHz (Fig. 3 D). When 5 mol % amantadine was incorporated into the lipid bilayers, the ^{31}P CSA increased to 56 ppm (Fig. 3 B), and the ^{14}N quadrupolar splitting decreased to 8 kHz (Fig. 3 E). When the amantadine mole fraction was increased to 10%, the ^{31}P CSA continued to increase to 60 ppm (Fig. 3 C), and ^{14}N quadrupolar splitting decreased to 7 kHz (Fig. 3 F). It is clearly shown that amantadine affects the headgroup orientation and/or dynamics in this concentration range, which is considerably higher than that under pharmaceutical conditions. Here the high concentration was used to help identify the location of amantadine within the membrane. The relatively large ^{14}N quadrupolar coupling constant of the amantadine amine group was not observed here. It has previously been shown that the features of ^{31}P and ^{14}N anisotropy are sensitive to variations in the DMPC surface potential (35–37). Our results suggest that the P- N^+ dipole orientation changes on incorporation of amantadine and

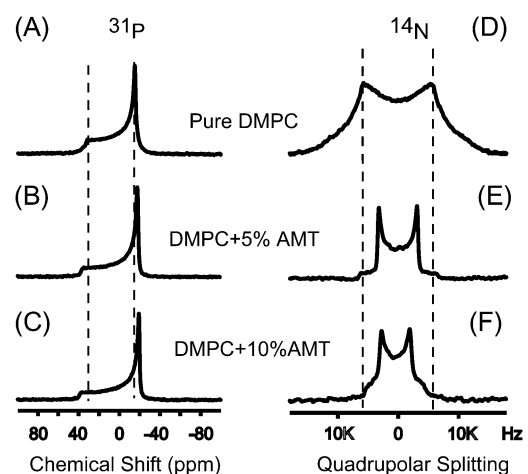


FIGURE 3 Static ^{31}P spectra (left column) from a 300-MHz spectrometer and ^{14}N spectra from an 830-MHz spectrometer (right column) of randomly oriented hydrated DMPC in the presence of amantadine in mole percent: 0% (A and D), 5% (B and E), and 10% (C and F) amantadine. The experiments were performed at 30°C and pH 8.0.

hence changes the surface potential at these high amantadine concentrations.

Location of the amantadine in the DMPC bilayers

Fig. 4 displays ^{31}P and ^{15}N spectra of aligned DMPC/amantadine samples (molar ratio 20:1) in the absence (Fig. 4, A and C) and in the presence of 1.5 mol % Mn^{2+} . The ^{31}P resonance around 36 ppm (Fig. 4 A) demonstrates that the lipid bilayers are well aligned. This signal was barely observable when 1.5% Mn^{2+} was added to the sample because of the broadening induced by the paramagnetic relaxation enhancement of Mn^{2+} interacting with the membrane surface. However, the amantadine ^{15}N signal at 50 ppm (Fig. 4 C) was still observed in the same sample that showed no ^{31}P signal, although the intensity was greatly decreased. Note that in these spectra the ^{15}N signal from the DMPC choline site was not observed because of the low natural abundance and fast motion leading to poor cross-polarization efficiency. These observations suggest that the nitrogen atom of amantadine is less accessible to Mn^{2+} than the phosphates of DMPC.

Mn^{2+} is often employed as a paramagnetic relaxation agent to detect the insertion depth of lipophilic ligands in model membranes (38,39). It binds at the membrane surface (i.e., the phosphates) and dephases the lipid ^{13}C signals monotonically with increasing distance of the lipid methylene groups from the membrane surface. Thus, comparison of the intensity of amantadine carbons with that of the lipid carbons permits the relative depth of the amantadine with respect to the lipid moieties to be extracted. The ^{13}C CP-MAS spectra of amantadine in the DMPC lipid bilayers at different concentrations of Mn^{2+} and the amantadine resonance assignments from literature values (40) are shown in Fig. 5. With amantadine partitioned into DMPC bilayers, the chemical shifts of the amantadine resonances labeled with asterisks appear to be only slightly shifted in frequency, but their line width is much narrower when a dry powder of amantadine (Fig. 5 A) is dissolved into the bilayers (Fig. 5 B).

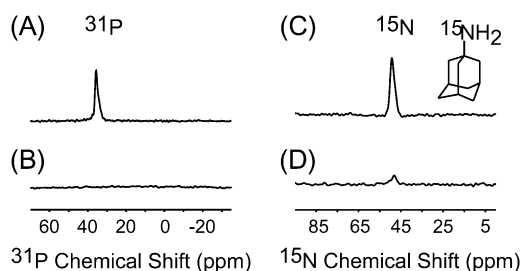


FIGURE 4 Static ^{31}P spectra (left column) from a 300-MHz spectrometer of DMPC and ^{15}N spectra (right column) from a 400-MHz spectrometer of amantadine (AMT/lipid, 1:20 molar ratio) in aligned hydrated DMPC bilayers (parallel with B_0) in the presence of Mn^{2+} in mole percent: 0% (A and C) and 1.5% Mn^{2+} (B and D). The experiments were performed at 30°C and pH 8.0.

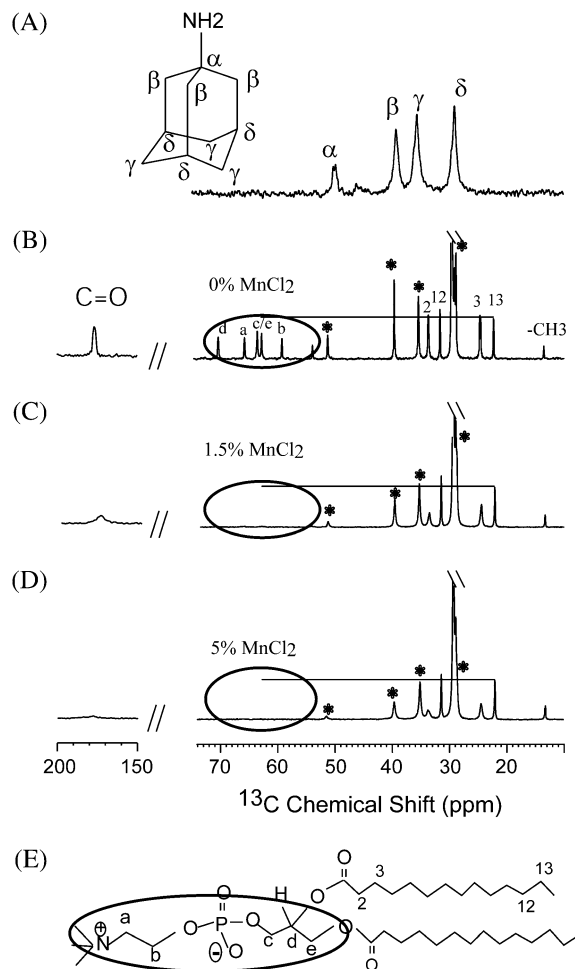


FIGURE 5 ^{13}C CP-MAS spectra of (A) dry powder sample of amantadine (the free base form, the molecule is shown to the left and the resonance assignments are labeled in the spectrum). (B) Amantadine in hydrated DMPC lipid bilayers: the signals from amantadine are labeled with asterisks. (C) The same sample as in B in the presence of 1.5% mol % MnCl_2 . (D) The same sample as in B in the presence of 5 mol % MnCl_2 . The experiments were performed at 30°C and pH 8.0. The molar ratio of amantadine to lipid is 1:5.

To simplify the interpretation, resonances of the lipid headgroup are circled and identified in Fig. 5 E. When 1.5% Mn^{2+} is present (Fig. 5 C), the lipid headgroup signals are no longer observable because of the broadening effect of Mn^{2+} ; however, the carbonyl carbon from the fatty acyl chain is still observable, though broadened. Similarly, the signal from the amantadine α -carbon is broadened but to a lesser extent than the β -carbons. In the presence of 5% Mn^{2+} (Fig. 5 D), the intensities of amantadine and most of the lipid signals decrease substantially except for the C12, C13, and methyl signals, which are in the bilayer center and are not influenced by Mn^{2+} . Therefore, by comparing the dephasing rate of amantadine signals using the ^{13}C resonance of the lipid as a reference intensity, it can be deduced that the amantadine signals dephase at rates $\alpha > \beta > \gamma$, suggesting that the C_α is closer to Mn^{2+} at the bilayer surface than the C_γ . This

observation implies that the amine group of amantadine is directed toward the bilayer surface, whereas the C_{γ}/C_{δ} end of amantadine is toward the bilayer center, as would be expected. More specifically, the data show that the C_{α} of amantadine has a similar dephasing rate as that of the carbonyl carbon of DMPC, suggesting that the two carbons are located at a similar depth in the membrane.

MD simulation

The alignment of amantadine in DMPC bilayer

Throughout the whole 12.6-ns simulation, amantadine remained in the upper leaflet of the membrane bilayer (Fig. 6). The average surface area per DMPC lipid of $59.4 \pm 0.6 \text{ \AA}^2$ over the last 10 ns of the trajectory is consistent with experimental observations (41,42). The alignment of amantadine in the DMPC bilayer was measured by the angle between the amantadine C_{α} -N vector and the membrane normal (Fig. 7, *black*). Consistent with the NMR data presented earlier, amantadine is oriented in the upright direction in the simulation, with the most probable tilt of 30° between the C_{α} -N vector and the membrane normal (Fig. 7, *red*).

Location of amantadine in DMPC bilayer

In agreement with the NMR data, as shown in Fig. 8, during the simulation the amantadine amine resides mainly between the phosphate and carbonyl groups of DMPC, with distances of the amine from the central plane of the membrane ranging from 11.7 \AA to 18.3 \AA for 90% of the time. For reference, the average distances of the choline, phosphate, and carbonyl groups over the 34 DMPC lipid molecules in the upper leaflet are also shown in Fig. 8. Although the average location of the headgroups in the bilayer is very stable, the headgroups of

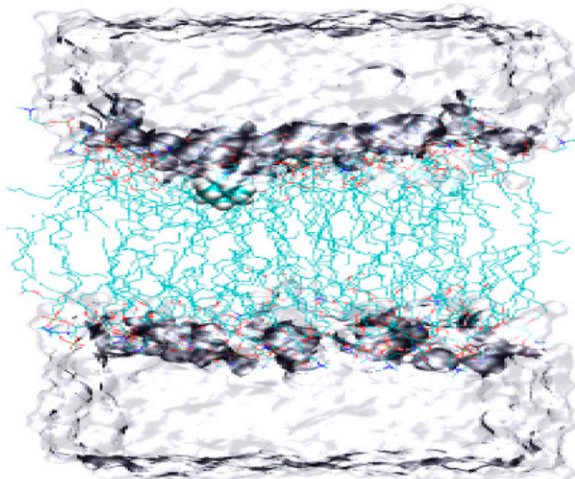


FIGURE 6 The membrane-amantadine-water system in MD simulation. DMPC lipid molecules, amantadine, and water box are represented by line, sphere, and surface, respectively.

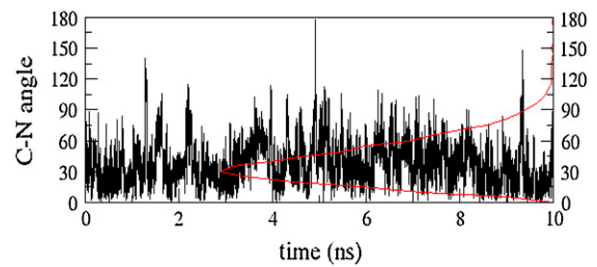


FIGURE 7 The angle of amantadine C_{α} -N vector to the membrane normal along the 10-ns trajectory (*black*) and its distribution with the peak at 30° (*red*).

the individual lipid molecules vary widely along the direction of the membrane normal. Minimum and maximum distances of the choline, phosphate, and carbonyl groups from the central plane through the 10-ns trajectory were 9 to 29, 10 to 26, and 3 to 22 \AA , respectively. Such limits of a dynamic range were not observed by NMR experiments because of the rarity of the event and the small population. The hydrophilic interfacial region of the bilayer was thus quite fluid, explaining the wide range of amantadine amine distances from the central plane (Fig. 8, *red*).

Influence of amantadine on the DMPC headgroup orientation

Interactions between amantadine and DMPC lipids influence the conformation of the lipids. The average angle of P-N dipoles to the bilayer normal in the DMPC headgroups near amantadine (Fig. 9, *green*) was different from those away from amantadine (Fig. 9, *blue*) in the upper leaflet. Interestingly, the average angle of the headgroup dipoles near amantadine is correlated with the depth of amantadine in the bilayer during the 10-ns trajectory (Fig. 8). When the

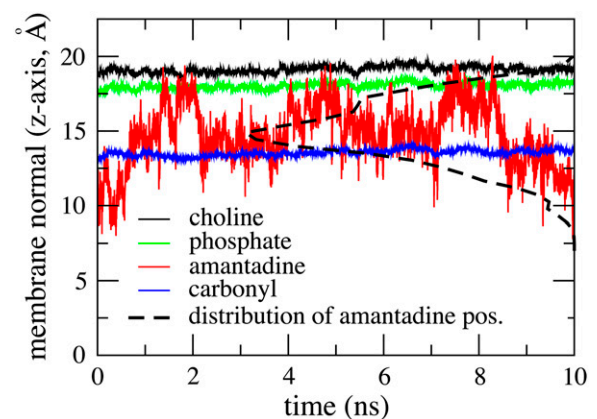


FIGURE 8 The relative depth of the amantadine (*red*, nitrogen atom) with respect to the DMPC lipid molecules in the upper leaflet. Distances from the bilayer central plane (0 \AA) along the 10-ns trajectory are shown. For comparison, the average distance of nitrogen (*black*), phosphorus (*green*), and oxygen (*blue*) atoms in choline, phosphate, and carbonyl groups from the membrane center are shown as well. The broken black line shows the distribution of the amantadine amine location with a peak at 15 \AA .

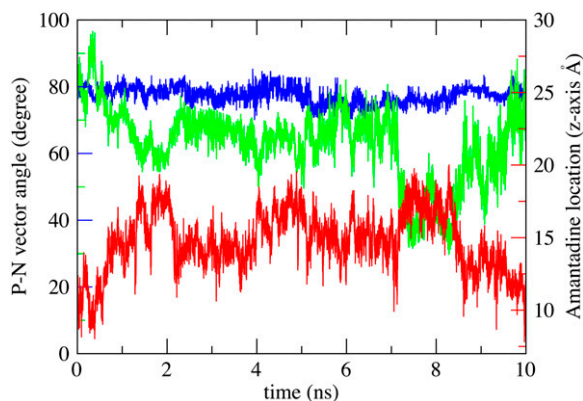


FIGURE 9 The average angle of DMPC P-N vectors in the upper leaflet with respect to the membrane normal, within 12 Å of amantadine (*green*) and that of the outside lipid molecules (*blue*) along the 10-ns trajectory. Amantadine location (*red*) and P-N angle (*green*) show an anti-correlation.

amantadine amine had the same depth as the phosphate and choline groups (around 2, 5, and 8 ns), the average angle of the P-N vectors from the bilayer normal was smaller (30° to 60°); in contrast, at the beginning and end of the 10-ns trajectory, when the amantadine amine was below the level of the carbonyl groups, the P-N angle increased ($\sim 80^\circ$) to that for the lipid molecules distant from amantadine. The large P-N angles are thought to be caused by intramolecular interactions between choline and carbonyl groups within the DMPC molecules (43). Amantadine appears to disrupt these intramolecular interactions when the amine interacts with the lipid headgroup. This influence on the P-N vector is likely to correspond with the change in the average P-N⁺ dipole orientation observed by NMR.

Influence of amantadine on lipid acyl chains

Details of the amantadine-membrane interactions were further analyzed. Heavy atoms of DMPC lipid molecules within 4 Å of amantadine were identified in each snapshot along the 10-ns trajectory. Based on this 4 Å criterion, amantadine on average interacted with 3.6 lipid molecules simultaneously, involving 8.3 heavy atoms of the lipids. Amantadine interacted with the carbonyl groups 94% of the time, with the phosphate groups 72% of the time, and with acyl chains 87% of the time. Inspection of the conformations of the surrounding lipid molecules revealed that their acyl chains were bent to fill in the space below amantadine; the acyl chains effectively wrapped around the bottom of amantadine. A representative snapshot showing the conformations of lipids around amantadine is presented in Fig. 10. This detailed picture from the MD simulation, with the amantadine amine located around the phosphate and carbonyl groups but with acyl chains curled up to wrap around the bottom of the drug molecule, indicates how amantadine can interact with the lipid headgroups and the distal end of the fatty acyl chains at the same time.

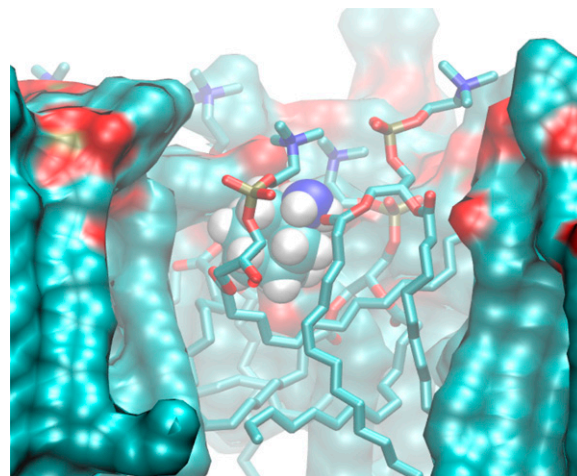


FIGURE 10 A snapshot of the MD simulation at 3.8 ns from the beginning of 10-ns trajectory. Lipids around and away from amantadine in the upper leaflet are shown by stick and surface representations, respectively. Amantadine is represented by spheres. Carbon, nitrogen, oxygen, hydrogen, and phosphorus atoms are colored in cyan, blue, red, white, and brown, respectively.

DISCUSSION

The results from this work build on a considerable literature using various techniques to characterize amantadine interactions with model membranes. Chou and co-workers (18) have elegantly characterized the partition coefficient for amantadine into a DMPC bilayer environment through the use of soluble bicelle samples. Here, the solid-state NMR data and simulation results indicate that amantadine partitions into the membrane with a preferred equilibrium location in the interfacial region, such that the amine can be in a relatively hydrophilic domain and the amantadine hydrocarbon can be in the hydrophobic region of the bilayer. This is similar to the equilibrium position for tryptophan side chains of membrane proteins (44,45). Amantadine is a weak base with a pK_a of 9 determined in aqueous solution (46), but it is well known that pK_a s can change by several pH units for titratable sites that interact with a membrane environment (47,48). The ^{15}N powder pattern results clearly show that, under the conditions used here, we are observing the uncharged amine at pH 8 and the charged amine at pH 2, where no significant chemical shift anisotropy is observed.

Interestingly, the ^{31}P chemical shift anisotropy, which was shown here to increase in magnitude when amantadine was added to DMPC bilayers, is the opposite of what was observed by Epand and co-workers (49) when they added amantadine to bilayers of dielaidoylphosphatidylethanolamine (DEPE). This is likely caused by the high sensitivity of the ^{31}P CSA to the phospholipid headgroup orientation and the very different headgroup conformation for PE and PC. Although mixed phases have been characterized by ^{31}P CSA for amantadine preparations at elevated temperature,

there was no evidence here that amantadine induced a nonbilayer DMPC phase at 30°C.

Previous studies of the influence of amantadine on lipid bilayers have generated confusing conclusions about the location of amantadine within the lipid bilayer. Neutron and x-ray diffraction results led to a proposal that the uncharged amantadine had two populations, one that was nearly at the bilayer center and one at the water/bilayer interface (17). This proposal was further supported by EPR studies of spin-labeled amantadine (19). Both the experimental and computational results reported here suggest that there is a single homogeneous, although dynamic, population in the membrane. The location of amantadine along the normal to the bilayer appears to be between the two populations described from the diffraction study.

Chou and co-workers (18) have used NMR experiments to transfer magnetization from the lipid environment to the C γ -H sites of amantadine to qualitatively assess the location of the drug within bicelles. Although they showed no transfer from the choline methyls, there was transfer from the glycerol backbone and the entire fatty acyl chain to amantadine. Here, it was shown that all of the amantadine resonances were influenced by the water-soluble Mn²⁺ relaxation agent, whereas the terminal carbons on the fatty acyl chains were not affected. The computational results showed rotational excursions of the amantadine that might expose the γ and δ carbons occasionally to the hydrophilic surface, explaining the induced relaxation by Mn²⁺ and the saturation transfer results from the glycerol backbone to the C γ -H sites on amantadine. Although the terminal carbons of the fatty acyl chains remain far removed from the hydrophilic surface and the Mn²⁺ relaxation agent, our simulation results show that the fatty acyl chains wrap around the amantadine hydrocarbon moiety, potentially accounting for the close approach of the terminal methyl with amantadine C γ -H and thereby explaining the saturation transfer results with the terminal methyl groups. In addition, it may help to explain the diffraction results that suggested that there was a population of amantadine near the bilayer center. Here, the simulations show not only that the methyls can be close to amantadine but also how the bilayer can be significantly distorted, which may help to explain the diffraction data.

Consequently, the data from bicelles are consistent with those observed here in bilayers, although we would argue based on our observation of the amantadine amine that amantadine does interact with the bilayer surface. In addition to a preferred position in the membrane, amantadine has a preferred equilibrium orientation and does not tumble freely in the lipid bilayer. This is in contrast with the results from Wang et al. (18), which suggest that amantadine tumbles freely in the bicelle based on the observation of the same ¹H line width of amantadine in bicelles and in organic solvent. However, here it is clear that amantadine has a unique position, orientation, and dynamic amplitude in liquid crystalline lipid bilayers that do not permit it to cross the membrane, at least not

rapidly. The results here and in the literature suggest that the drug partitions extensively in the membrane and is bound at the hydrophilic/hydrophobic lipid interface. Although we believe that amantadine binds to M2 protein on its tetrameric symmetry axis, this suggests that amantadine binds to M2 protein via the small aqueous population of the drug. Furthermore, despite being lipophilic, amantadine does not appear to readily cross the bilayer center due to its interaction with the bilayer surface.

The authors acknowledge the support of National Institute of Allergy and Infectious Diseases (AI-23007). The NMR spectroscopy was performed at the National High Magnetic Field Lab supported through a cooperative agreement between the NSF (DMR-0084173) and the State of Florida.

REFERENCES

- Rhodes, D. G., J. G. Sarmiento, and L. G. Herbet. 1985. Kinetics of binding of membrane-active drugs to receptor sites. Diffusion-limited rates for a membrane bilayer approach of 1,4-dihydropyridine calcium channel antagonists to their active site. *Mol. Pharmacol.* 27:612–623.
- Pawlikowska-Pawlega, B., W. I. Gruszecki, L. E. Misiak, and A. Gawron. 2003. The study of the quercetin action on human erythrocyte membranes. *Biochem. Pharmacol.* 66:605–612.
- Makriyannis, A., X. Tian, and J. Guo. 2005. How lipophilic cannabinergic ligands reach their receptor sites. *Prostaglandins Other Lipid Mediat.* 77:210–218.
- Zhou, H. X., and A. Szabo. 2004. Enhancement of association rates by nonspecific binding to DNA and cell membranes. *Phys. Rev. Lett.* 93:178101.
- Holsinger, L. J., and R. A. Lamb. 1991. Influenza virus M2 integral membrane protein is a homotetramer stabilized by formation of disulfide bonds. *Virology.* 183:32–43.
- Takeda, M., A. Pekosz, K. Shuck, L. H. Pinto, and R. A. Lamb. 2002. Influenza A virus M2 ion channel activity is essential for efficient replication in tissue culture. *J. Virol.* 76:1391–1399.
- Pinto, L. H., L. J. Holsinger, and R. A. Lamb. 1992. Influenza virus M2 protein has ion channel activity. *Cell.* 69:517–528.
- Chizhmakov, I. V., F. M. Geraghty, D. C. Ogden, A. Hayhurst, M. Antoniou, and A. J. Hay. 1996. Selective proton permeability and pH regulation of the influenza virus M2 channel expressed in mouse erythroleukaemia cells. *J. Physiol.* 494:329–336.
- Vijayvergiya, V., R. Wilson, A. Chorak, P. F. Gao, T. A. Cross, and D. D. Busath. 2004. Proton conductance of influenza virus M2 protein in planar lipid bilayers. *Biophys. J.* 87:1697–1704.
- Wang, C., K. Takeuchi, L. H. Pinto, and R. A. Lamb. 1993. Ion channel activity of influenza A virus M2 protein: characterization of the amantadine block. *J. Virol.* 67:5585–5594.
- Skehel, J. J. 1992. Influenza virus. Amantadine blocks the channel. *Nature.* 358:110–111.
- Duff, K. C., and R. H. Ashley. 1992. The transmembrane domain of influenza-A M2 protein forms amantadine-sensitive proton channels in planar lipid bilayers. *Virology.* 190:485–489.
- Hu, J., R. Fu, K. Nishimura, L. Zhang, H. X. Zhou, D. D. Busath, V. Vijayvergiya, and T. A. Cross. 2006. Histidines, heart of the hydrogen ion channel from influenza A virus: toward an understanding of conductance and proton selectivity. *Proc. Natl. Acad. Sci. USA.* 103:6865–6870.
- Hu, J., T. M. Asbury, S. Achuthan, C. Li, R. Bertram, J. R. Quine, R. Fu, and T. A. Cross. 2007. Backbone structure of the amantadine-blocked trans-membrane domain M2 proton channel from influenza A virus. *Biophys. J.* 92:4335–4343.
- Fieschi, C., M. Nardini, M. Casacchia, and M. E. Tedone. 1970. Amantadine for Parkinson's disease. *Lancet.* 1:945–946.

16. Blanchet, P. J., L. V. Metman, and T. N. Chase. 2003. Renaissance of amantadine in the treatment of Parkinson's disease. *Adv. Neurol.* 91: 251–257.
17. Duff, K. C., A. J. Cudmore, and J. P. Bradshaw. 1993. The location of amantadine hydrochloride and free base within phospholipid multilayers—a neutron and x-ray-diffraction study. *Biochim. Biophys. Acta.* 1145:149–156.
18. Wang, J. F., J. R. Schnell, and J. J. Chou. 2004. Amantadine partition and localization in phospholipid membrane: a solution NMR study. *Biochem. Biophys. Res. Commun.* 324:212–217.
19. Subczynski, W. K., J. Wojas, V. Pezeshk, and A. Pezeshk. 1998. Partitioning and localization of spin-labeled amantadine in lipid bilayers: An EPR study. *J. Pharm. Sci.* 87:1249–1254.
20. Stetter, H., J. Mayer, M. Schwarz, and K. Wulff. 1960. Über Verbindungen Mit Urotropin-Struktur. 16. Beitrage Zur Chemie Der Adamantyl-(1)-Derivate. *Chemische Berichte-Recueil.* 93:226–230.
21. Davis, J. H., K. R. Jeffrey, M. Bloom, M. I. Valic, and T. P. Higgs. 1976. Quadrupolar echo deuterium magnetic resonance spectroscopy in ordered hydrocarbon chains. *Chem. Phys. Lett.* 42:390–394.
22. Case, D. A., T. A. Darden, T. E. I. Cheatham, C. L. Simmerling, J. Wang, R. E. Duke, R. Luo, K. M. Merz, B. Wang, D. A. Pearlman, M. Crowley, S. Brozell, V. Tsui, H. Gohlke, J. Mogan, V. Hornak, G. Cui, P. Beroza, C. Schafmeister, J. W. Caldwell, W. S. Ross, and P. A. Kollman. 2004. AMBER 8. University of California, San Francisco.
23. Feller, S. E., and A. D. MacKerell. 2000. An improved empirical potential energy function for molecular simulations of phospholipids. *J. Phys. Chem. B.* 104:7510–7515.
24. Frisch, M. J. T. G. W., H. B. Schlegel, G. E. Scuseria, M. A. Robb, J. R. Cheeseman, J. Montgomery, J. A., T. Vreven, K. N. Kudin, J. C. Burant, J. M. Millam, S. S. Iyengar, J. Tomasi, V. Barone, B. Mennucci, M. Cossi, G. Scalmani, N. Rega, G. A. Petersson, H. Nakatsuji, M. Hada, M. Ehara, K. Toyota, R. Fukuda, J. Hasegawa, M. Ishida, T. Nakajima, Y. Honda, O. Kitao, H. Nakai, M. Klene, X. Li, J. E. Knox, H. P. Hratchian, J. B. Cross, V. Bakken, C. Adamo, J. Jaramillo, R. Gomperts, R. E. Stratmann, O. Yazyev, A. J. Austin, R. Cammi, C. Pomelli, J. W. Ochterski, P. Y. Ayala, K. Morokuma, G. A. Voth, P. Salvador, J. J. Dannenberg, V. G. Zakrzewski, S. Dapprich, A. D. Daniels, M. C. Strain, O. Farkas, D. K. Malick, A. D. Rabuck, K. Raghavachari, J. B. Foresman, J. V. Ortiz, Q. Cui, A. G. Baboul, S. Clifford, J. Cioslowski, B. B. Stefanov, G. Liu, A. Liashenko, P. Piskorz, I. Komaromi, R. L. Martin, D. J. Fox, T. Keith, M. A. Al-Laham, C. Y. Peng, A. Nanayakkara, M. Challacombe, P. M. W. Gill, B. Johnson, W. Chen, M. W. Wong, C. Gonzalez, and J. A. and Pople. 2004. Gaussian 03, Revision C.02. Gaussian, Wallingford, CT.
25. Wang, J. M., P. Cieplak, and P. A. Kollman. 2000. How well does a restrained electrostatic potential (RESP) model perform in calculating conformational energies of organic and biological molecules? *J. Comput. Chem.* 21:1049–1074.
26. Wang, J. M., R. M. Wolf, J. W. Caldwell, P. A. Kollman, and D. A. Case. 2004. Development and testing of a general amber force field. *J. Comput. Chem.* 25:1157–1174.
27. Berendsen, H. J. C., J. P. M. Postma, W. F. Vangunsteren, A. Dinola, and J. R. Haak. 1984. Molecular-Dynamics with Coupling to an External Bath. *J. Chem. Phys.* 81:3684–3690.
28. Darden, T., D. York, and L. Pedersen. 1993. Particle Mesh Ewald - an N.Log(N) Method for Ewald Sums in Large Systems. *J. Chem. Phys.* 98:10089–10092.
29. Essmann, U., L. Perera, M. L. Berkowitz, T. Darden, H. Lee, and L. G. Pedersen. 1995. A Smooth Particle Mesh Ewald Method. *J. Chem. Phys.* 103:8577–8593.
30. Toukmaji, A., C. Sagui, J. Board, and T. Darden. 2000. Efficient particle-mesh Ewald based approach to fixed and induced dipolar interactions. *J. Chem. Phys.* 113:10913–10927.
31. Miyamoto, S., and P. A. Kollman. 1992. Settle - an Analytical Version of the Shake and Rattle Algorithm for Rigid Water Models. *J. Comput. Chem.* 13:952–962.
32. Ryckaert, J. P., G. Ciccotti, and H. J. C. Berendsen. 1977. Numerical-integration of Cartesian equations of motion of a system with constraints—molecular-dynamics of N-alkanes. *J. Comput. Phys.* 23: 327–341.
33. Jorgensen, W. L., J. Chandrasekhar, J. D. Madura, R. W. Impey, and M. L. Klein. 1983. Comparison of Simple Potential Functions for Simulating Liquid Water. *J. Chem. Phys.* 79:926–935.
34. Bastug, T., and S. Kuyucak. 2005. Test of molecular dynamics force fields in gramicidin A. *Eur. Biophys. J.* 34:377–382.
35. Lindstrom, F., P. T. Williamson, and G. Grobner. 2005. Molecular insight into the electrostatic membrane surface potential by $^{14}\text{N}/^{31}\text{P}$ MAS NMR spectroscopy: nociceptin-lipid association. *J. Am. Chem. Soc.* 127:6610–6616.
36. Santos, J. S., D. K. Lee, and A. Ramamoorthy. 2004. Effects of anti-depressants on the conformation of phospholipid headgroups studied by solid-state NMR. *Magn. Reson. Chem.* 42:105–114.
37. Rothgeb, T. M., and E. Oldfield. 1981. Nitrogen-14 nuclear magnetic resonance spectroscopy as a probe of lipid bilayer headgroup structure. *J. Biol. Chem.* 256:6004–6009.
38. Buffry, J. J., T. Hong, S. Yamaguchi, A. J. Waring, R. I. Lehrer, and M. Hong. 2003. Solid-state NMR investigation of the depth of insertion of protegrin-1 in lipid bilayers using paramagnetic Mn^{2+} . *Biophys. J.* 85:2363–2373.
39. Tuzi, S., J. Hasegawa, R. Kawaminami, A. Naito, and H. Saito. 2001. Regio-selective detection of dynamic structure of transmembrane α -helices as revealed from (^{13}C) NMR spectra of $[3\text{-}^{13}\text{C}]\text{Ala}$ -labeled bacteriorhodopsin in the presence of Mn^{2+} ion. *Biophys. J.* 81:425–434.
40. Lee, C. W., and R. G. Griffin. 1989. Two-dimensional $^1\text{H}/^{13}\text{C}$ heteronuclear chemical shift correlation spectroscopy of lipid bilayers. *Biophys. J.* 55:355–358.
41. Petrache, H. I., S. Tristram-Nagle, and J. F. Nagle. 1998. Fluid phase structure of EPC and DMPC bilayers. *Chem. Phys. Lipids.* 95:83–94.
42. Koenig, B. W., H. H. Strey, and K. Gawrisch. 1997. Membrane lateral compressibility determined by NMR and x-ray diffraction: Effect of acyl chain polyunsaturation. *Biophys. J.* 73:1954–1966.
43. Pasenkiewicz-Gierula, M., Y. Takaoka, H. Miyagawa, K. Kitamura, and A. Kusumi. 1999. Charge pairing of headgroups in phosphatidylcholine membranes: A molecular dynamics simulation study. *Biophys. J.* 76:1228–1240.
44. Hu, W., K. C. Lee, and T. A. Cross. 1993. Tryptophans in membrane proteins: indole ring orientations and functional implications in the gramicidin channel. *Biochemistry.* 32:7035–7047.
45. Gaede, H. C., W. M. Yau, and K. Gawrisch. 2005. Electrostatic contributions to indole-lipid interactions. *J. Phys. Chem. B.* 109:13014–13023.
46. Spector, R. 1988. Transport of amantadine and rimantadine through the blood-brain barrier. *J. Pharmacol. Exp. Ther.* 244:516–519.
47. Cabral, D. J., J. A. Hamilton, and D. M. Small. 1986. The ionization behavior of bile acids in different aqueous environments. *J. Lipid Res.* 27:334–343.
48. Urry, D. W., S. Q. Peng, and T. M. Parker. 1992. Hydrophobicity-induced pK shifts in elastin protein-based polymers. *Biopolymers.* 32:373–379.
49. Epan, R. M., R. F. Epan, and R. C. McKenzie. 1987. Effects of viral chemotherapeutic agents on membrane properties. Studies of cyclosporin A, benzylloxycarbonyl-D-Phe-L-Phe-Gly and amantadine. *J. Biol. Chem.* 262:1526–1529.